Electronic Supplementary Material (ESI) for Materials Chemistry Frontiers.

Supporting Information

Regulation of Solid-state Dual-emission Properties by Switching Luminescent Processes Based on the Bis-*o*-carborane-modified Anthracene Triad

Kazuhiro Yuhara, Kazuo Tanaka* and Yoshiki Chujo

Department of Polymer Chemistry, Graduate School of Engineering, Kyoto University
Katsura, Nishikyo-ku, Kyoto 615-8510, Japan

E-mail: tanaka@poly.synchem.kyoto-u.ac.jp

General

^{1}H, ^{13}C, and ^{11}B NMR spectra were recorded on a JEOL JNM-AL400 instrument at 400, 100, and 128 MHz, respectively. The ^{1}H and ^{13}C chemical shift values were expressed relative to non-deuterated solvent in CD_2Cl_2 as an internal standard. The ^{11}B chemical shift values were expressed relative to $BF_3 \cdot Et_2O$ as an external standard. Analytical thin-layer chromatography (TLC) was performed with silica gel 60 Merck F254 plates. Column chromatography was performed with Wakogel® C-300 silica gel. High-resolution mass spectrometry (HRMS) was performed at the Technical Support Office (Department of Synthetic Chemistry and Biological Chemistry, Graduate School of Engineering, Kyoto University), and the HRMS spectra were obtained on a Thermo Fisher Scientific Exactive Plus for atomospheric pressure chemical ionization (APCI). UV–vis absorption and diffusion reflectance spectra were obtained on a SHIMADZU UV3600i plus spectrophotometer. Photoluminescence (PL) spectra were measured with a HORIBA JOBIN YVON Fluorolog-3 spectrofluorometer and an Oxford Optistat DN for temperature control. The fluorescence quantum yield (QY) was recorded on a HAMAMATSU Quantaurus-QY Plus C13534-01 model. The PL lifetime and time resolved emission spectra measurement was performed on a Horiba FluoroCube spectrofluorometer system; excitation was carried out using a UV diode laser (NanoLED 369 nm). The X-ray crystallographic analysis was carried out by a Rigaku Saturn 724+ with MicroMax-007 HF CCD diffractometer with Varimax Mo optics using graphite-monochromated Mo Kα radiation. The structures were solved with SHELXT 2015[1] and refined on F^2 with SHELXL 2015[2] on Olex 2-1.2.[3] All hydrogen atoms were placed at calculated positions and refined using a riding model. The program ORTEP-3[4] was used to generate the X-ray structural diagram. Thermogravimetric analyses (TGA) were performed by a HITACHI STA 7200RV instrument with the aluminum pan and the heating rate of 10 °C/min. up to 500 °C under nitrogen flow (200 mL/min). Differential scanning calorimetry (DSC) measurements were carried out on a HITACHI DSC 7020 instrument with the aluminum pan and the heating rate of 10 °C/min under nitrogen flow (50 mL/min). Powder X-ray diffraction (PXRD) data were collected with a Rigaku SmartLab Diffractometer (sealed tube (50 kV, 40 mA); Cu Kα, 1.542 Å; Bragg–Brentano geometry). PXRD samples were placed on a single-crystal silicon substrate.

Materials

Commercially available compounds used without purification

1,8-Diiodoanthracene, $B_{10}H_{14}$, *N*,*N*-dimethylaniline and polystyrene.

Commercially available solvents

Toluene, $CHCl_3$, CH_2Cl_2, MeOH, *n*-hexane, CCl_4, cyclohexane, $CDCl_3$ and CD_2Cl_2.

Compounds prepared as described in the literatures

1,8-Diethynylanthracene[5].

Synthetic Procedures

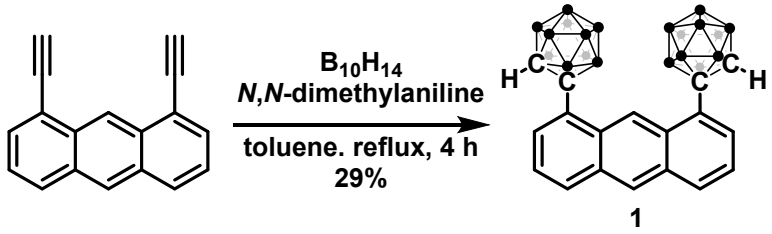

Scheme S1. Synthesis of **1**.

Synthesis of 1. Synthesis of **1** was performed according to Scheme S1. In the 100 mL round bottom flask, 1,8-diethynylanthracene (624 mg, 2.76 mmol), decaborane (779 mmol, 3.44 mmol) and *N*,*N*-dimethylaniline (1.25 mL, 9.90 mmol) were dissolved in toluene (27.6 mL) under N_2 atmosphere. The reaction mixture was stirred by magnetic stirrer and refluxed for 4.5 h. After filtration to remove any insoluble impurities, the solvent was removed by a rotary evaporator. The crude product was purified by column chromatography (eluent: CH_2Cl_2/*n*-hexane 1/5 (v/v)) to give a yellow solid. Recrystallization of the residual solid from CCl_4 at 60 °C afforded **1a** (80 mg, 0.17 mmol, 6% isolated yield) as a yellow solid and that from $CHCl_3$ at 60 °C afforded **1c** (369 mg, 0.63 mmol, 23% isolated yield) as a light-yellow solid. **1b** and **1d** were prepared by recrystallization of the crude product from toluene at 110 °C and cyclohexane at 85 °C, respectively. Both **1b** (14 mg, 0.03 mmol) and **1d** (41 mg, 0.07 mmol) were obtained as a light-yellow solid. ^{1}H NMR (400MHz, CD_2Cl_2): δ (ppm) 9.60 (s, 1H), 8.57 (s, 1H), 8.08 (d, J = 8.3 Hz, 2H), 7.94 (dd, J = 7.4, 0.9 Hz, 2H), 7.46 (dd, J = 8.2, 7.6 Hz, 2H), 4.81 (s, 2H), 3.77–1.63 (br, 20H). ^{13}C NMR (100 MHz, CD_2Cl_2): δ (ppm) 132.34, 132.10, 130.77, 130.64, 129.28, 128.59, 124.96, 119.86, 78.17, 62.07. ^{11}B NMR (128 MHz, CD_2Cl_2): –3.34, –8.44, –9.62, –10.89, –12.56, –13.84. HRMS (p-APCI): calcd. for $C_{18}H_{30}B_{20}$+Cl^- $[M+Cl]^-$ 501.3946, found 501.3950. Anal. Calcd for $C_{18}H_{30}B_{20}$: C, 46.73; H, 6.54. Found: C, 46.52; H, 6.60.

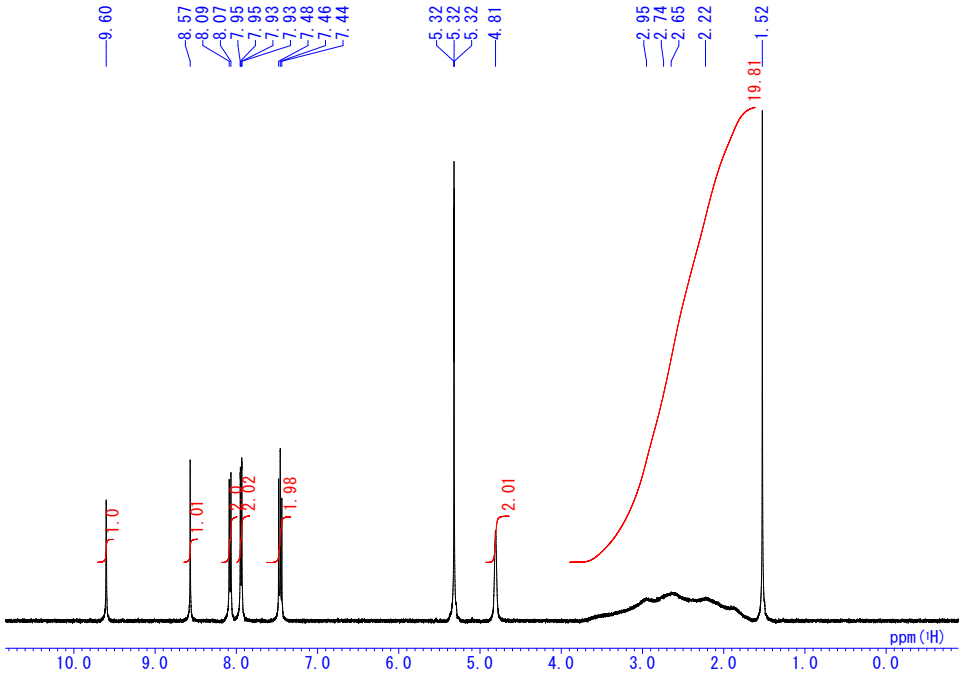

Chart S1. ^{1}H NMR spectrum of **1a** in CD_2Cl_2.

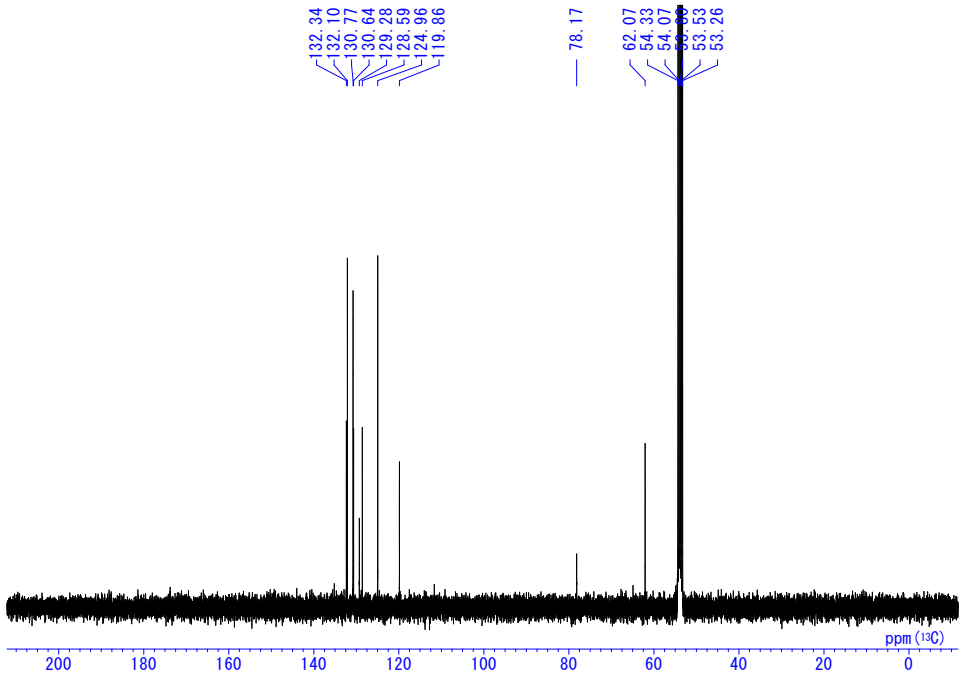

Chart S2. ^{13}C NMR spectrum of **1a** in CD_2Cl_2.

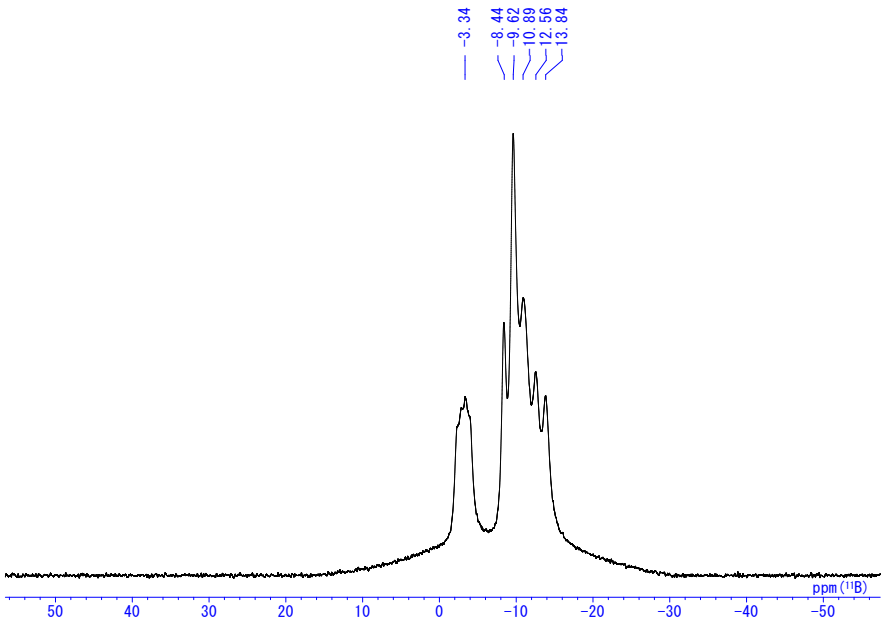

Chart S3. ^{11}B NMR spectrum of **1a** in CD_2Cl_2.

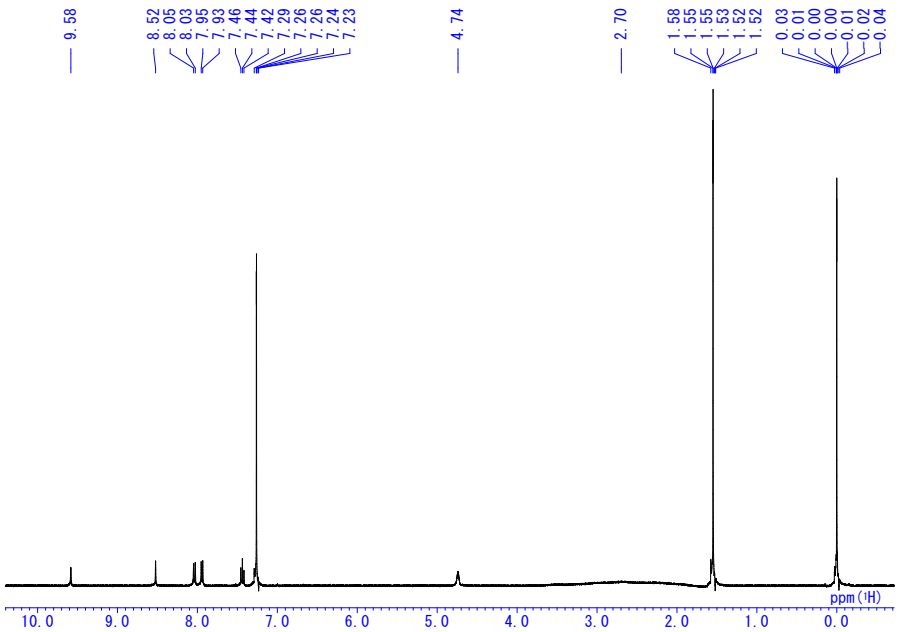

Chart S4. ^{1}H NMR spectrum of **1a** in $CDCl_3$.

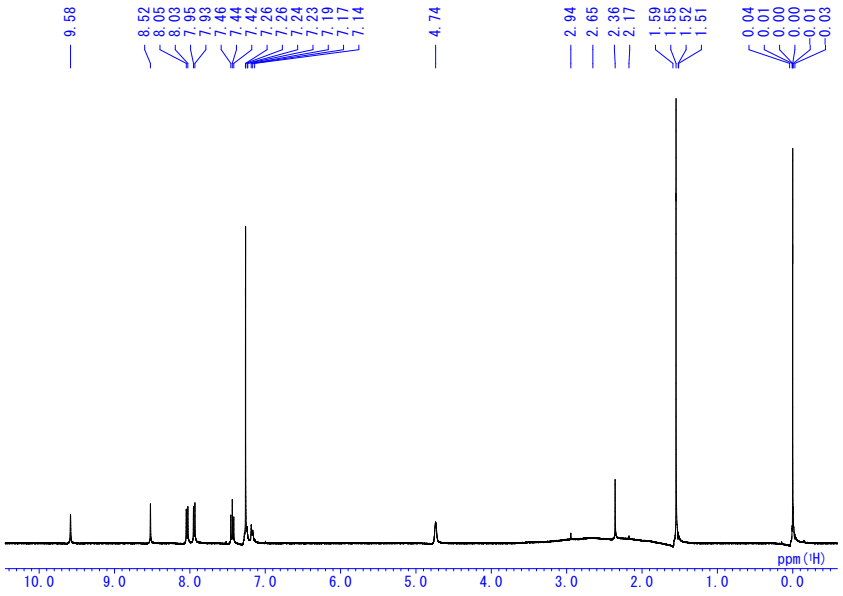

Chart S5. ^{1}H NMR spectrum of **1b** in $CDCl_3$.

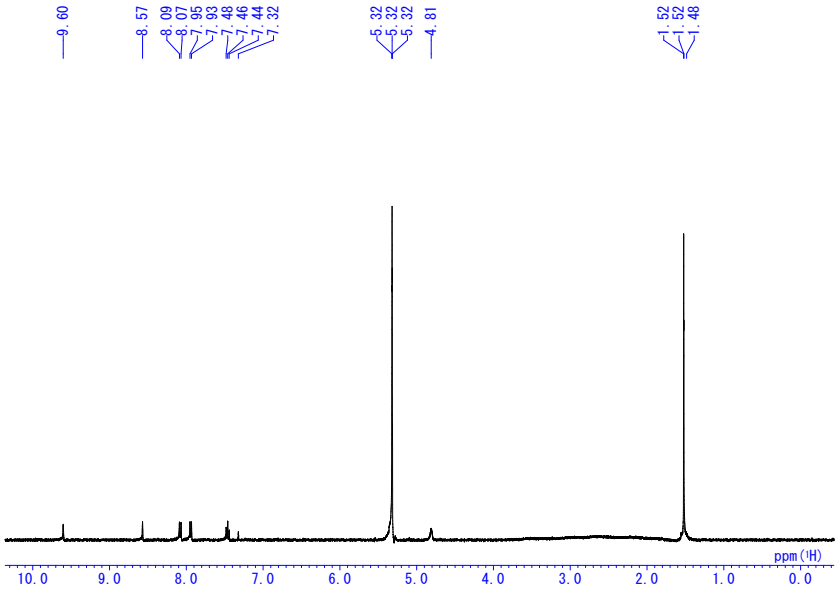

Chart S6. ^{1}H NMR spectrum of **1c** in CD_2Cl_2.

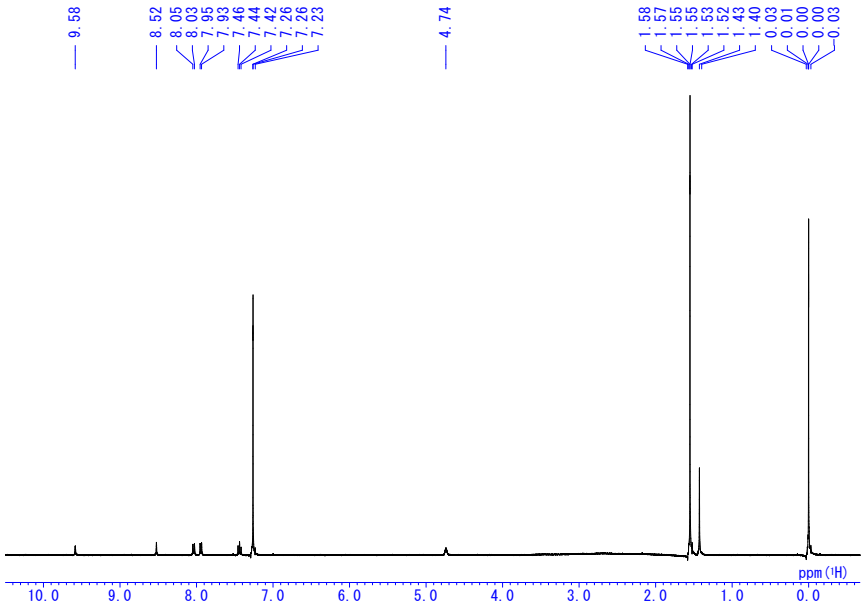

Chart S7. ^{1}H NMR spectrum of **1d** in $CDCl_3$.

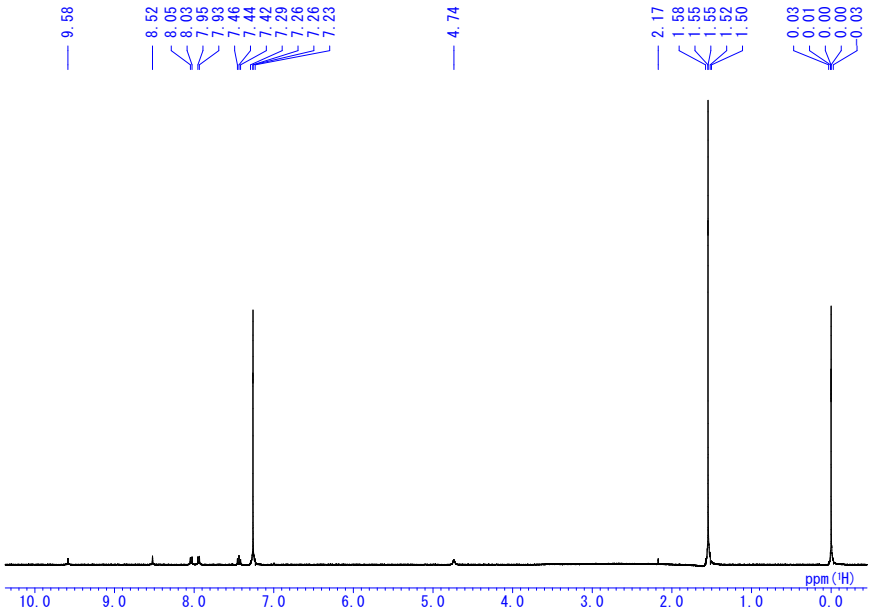

Chart S8. ^{1}H NMR spectrum of **1a** after heating in $CDCl_3$.

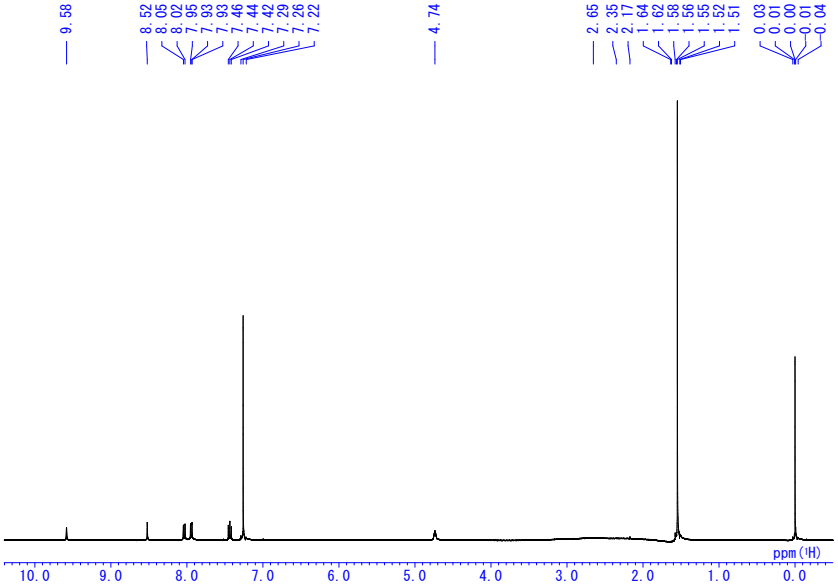

Chart S9. ^{1}H NMR spectrum of **1b** after heating in $CDCl_3$.

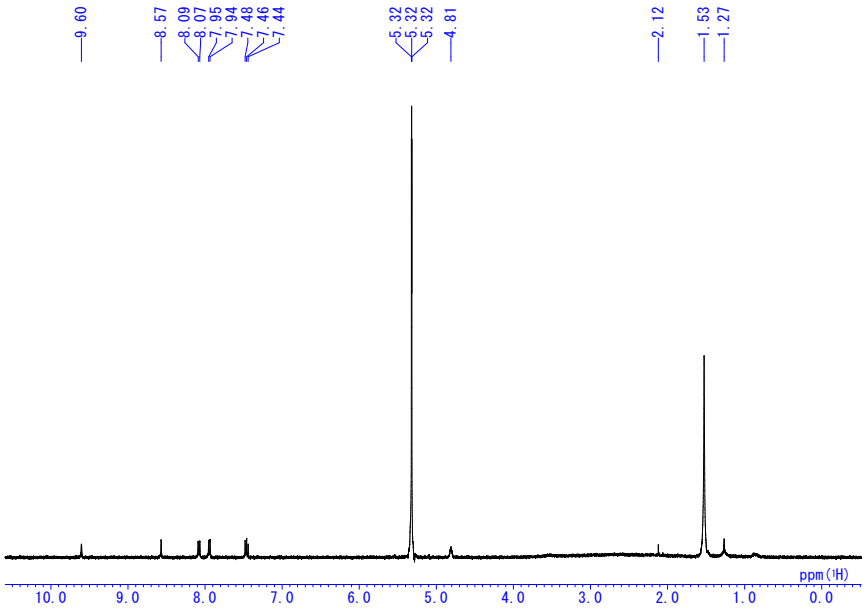

Chart S10. ^{1}H NMR spectrum of **1c** after heating in CD_2Cl_2.

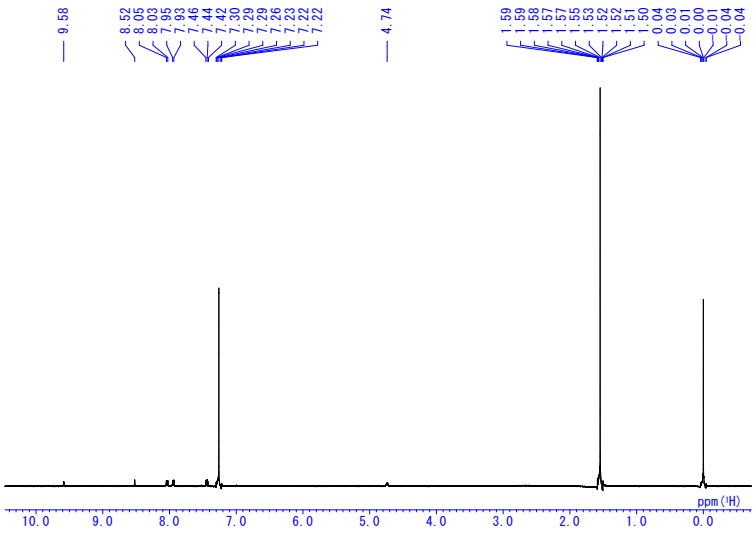

Chart S11. ^{1}H NMR spectrum of **1d** after heating in $CDCl_3$.

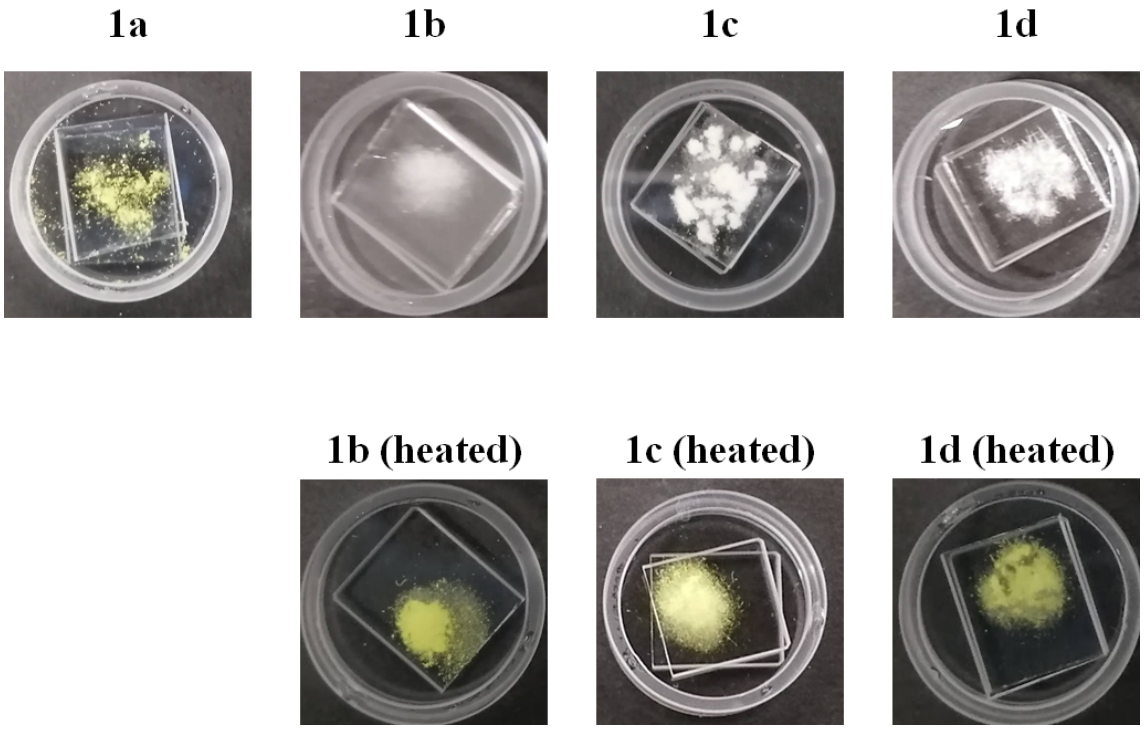

Figure S1. Appearances of **1a–1d** and **1b–1d** after heating at 200 ºC for 5 min.

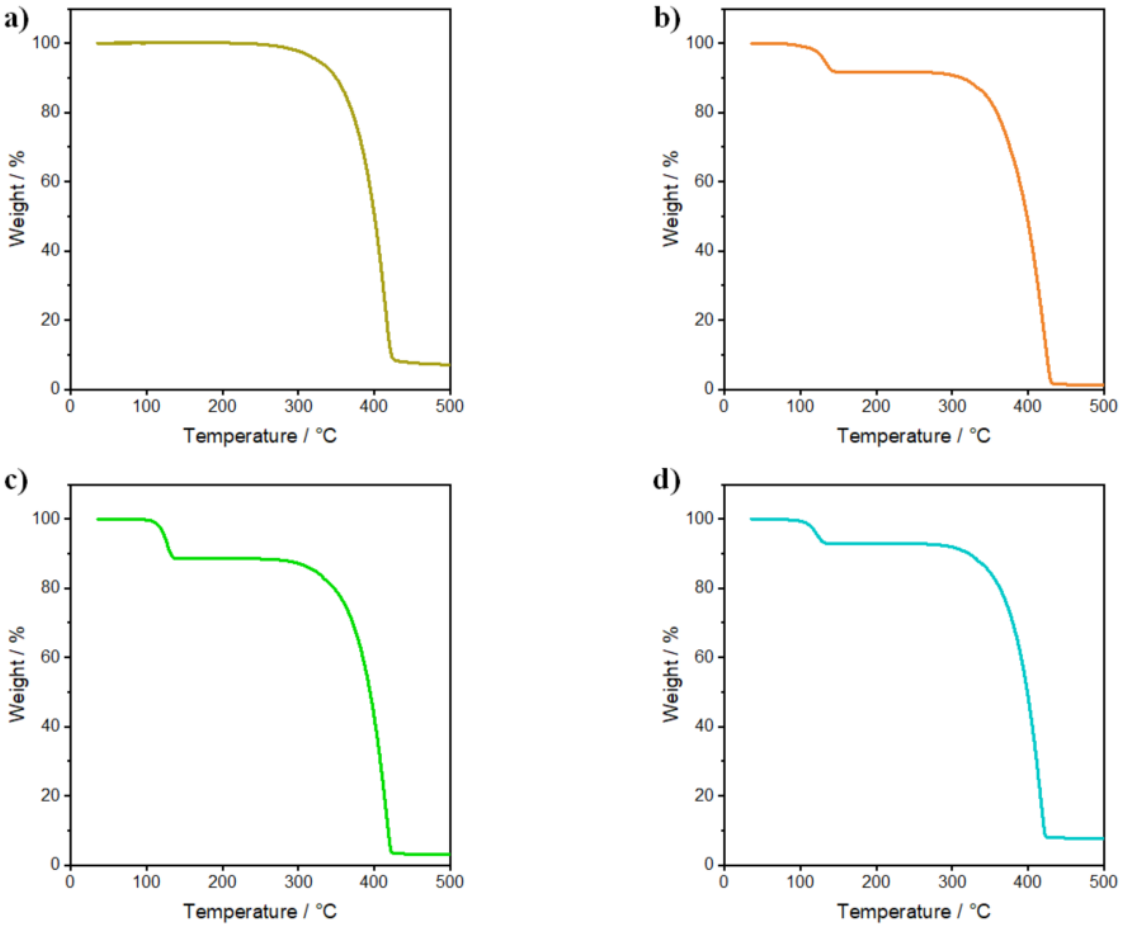

Figure S2. TGA profiles of **1a–1d** under nitrogen flow.

Table S1. Thermal properties of the crystal polymorphs

	1a	**1b**	**1c**	**1d**
T_p (ºC)[a]	n.d.[c]	156	129	143
T_d (ºC)[b]	377	372	375	376

[a]Phase transition temperature determined with DSC.

[b]Thermal degradation temperature determined with TGA.

[c]n.d. = not detected.

Table S2. The amount of the included solvents

	1b	**1c**	**1d**
SCXRD (molar ratio (**1**/solvent))[a]	0.50	–[c]	–[c]
TGA (molar ratio (**1**/solvent))[b]	0.45	0.48	0.42

[a]Determined with diffraction data of the single-crystal X-ray analysis.

[b]Determined with weight loss of the TGA.

[c]Single-crystal which is suitable for an X-ray analysis couldn't be obtained.

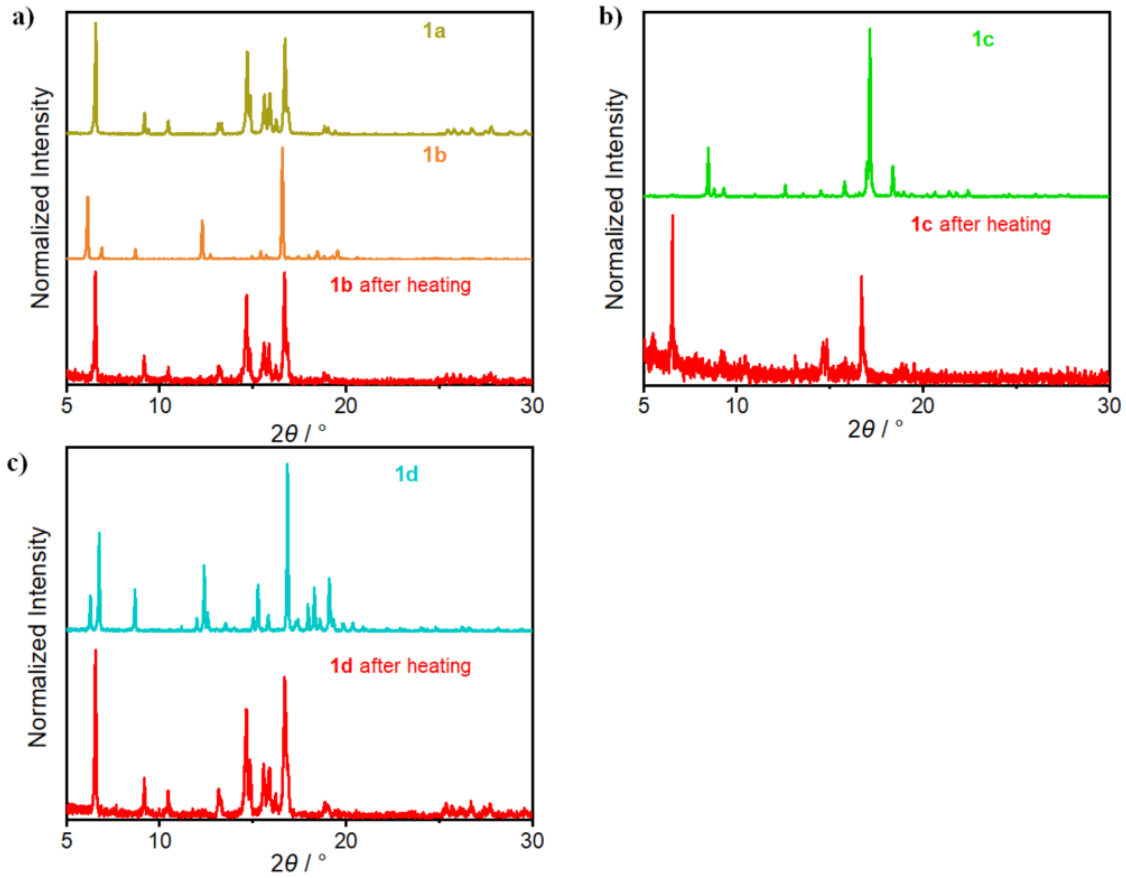

Figure S3. PXRD patterns of **1a**–**1d** before and after heating at 200 °C.

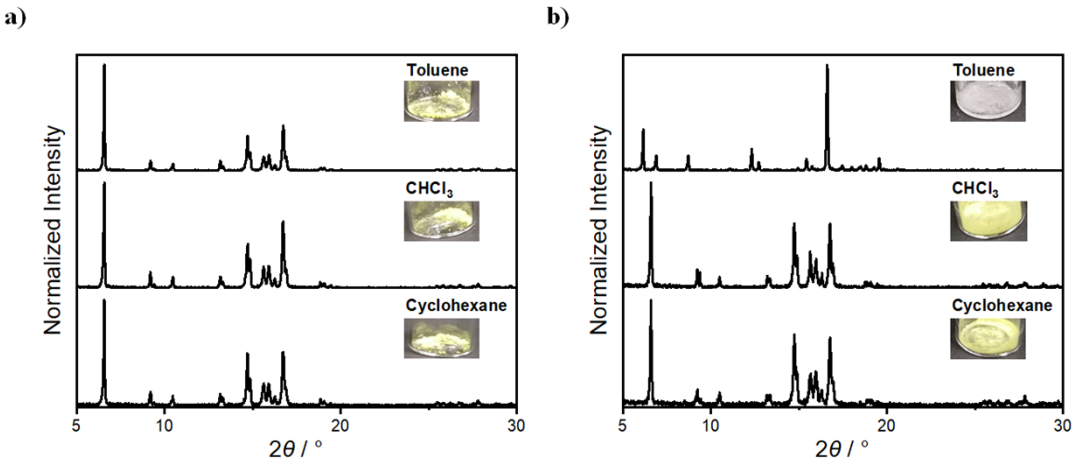

Figure S4. PXRD patterns of **1a** a) exposed to solvent vapor to 30 min and b) immersed to solvents. Inserted pictures are corresponding crystals after treatments.

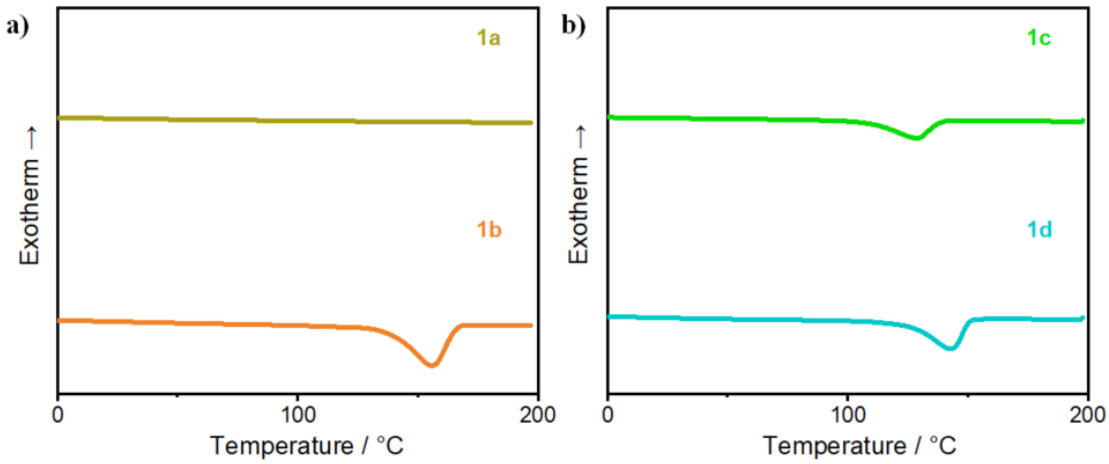

Figure S5. DSC profiles of **1a**–**1d**.

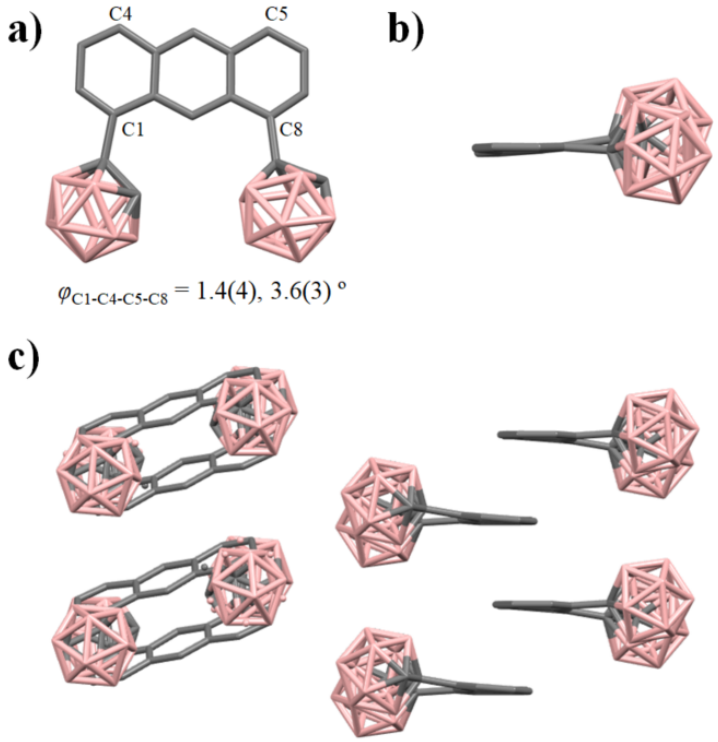

Figure S6. Crystal Structure of **1a**. a) Top, b) side views of molecular structure and c) Packing structure.

Table S3. Crystallographic data of **1a** (CCDC: 2155816)

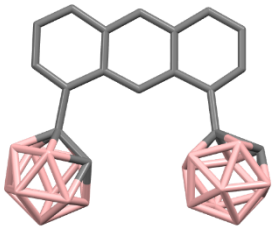

Empirical formula	$C_{18}H_{30}B_{20}$
Formula weight	462.62
Temperature (K)	143(2)
Wavelength (Å)	0.71075
Crystal system, space group	Triclinic, $P\bar{1}$
Unit cell dimensions	a = 7.115(6)
	b = 18.754(18)
	c = 19.216(16)
	α = 89.60(3)
	β = 83.73(4)
	γ = 87.73(3)
V (Å^3)	2547(4)
Z, calculated density (Mg m^{-3})	4, 1.207
Absorption coefficient	0.056
F(000)	952
Crystal size (mm)	0.20 × 0.06 × 0.06
θ range for data collection	3.042 – 27.464
Limiting indices	$-8 \le h \le 9$, $-23 \le k \le 24$, $-23 \le l \le 24$
Reflections collected (unique)	16814/2340 [R(int) = 0.1360]
Goodness-on-fit on F^2	0.971
Final R indices [$I > 2\sigma(I)$]	R_1 = 0.1751, wR_2 = 0.4055
R indices (all data)	R_1 = 0.2777, wR_2 = 0.4529

Table S4. Crystallographic data of **1b** (CCDC: 2155817)

Empirical formula	$C_{18}H_{30}B_{20}$
Formula weight	462.62
Temperature (K)	143(2)
Wavelength (Å)	0.71075
Crystal system, space group	monoclinic, $P2_1/c$
Unit cell dimensions	a = 6.926(3)
	b = 28.794(13)
	c = 14.201(7)
	α = 90
	β = 95.438(7)
	γ = 90
V (Å^3)	2819(2)
Z, calculated density (Mg m^{-3})	4, 1.090
Absorption coefficient	0.051
F(000)	952
Crystal size (mm)	0.17 × 0.09 × 0.01
θ range for data collection	3.038 –27.481
Limiting indices	$-8 \le h \le 8$, $-37 \le k \le 37$, $-18 \le l \le 18$
Reflections collected (unique)	22760/4770 [R(int) = 0.1429]
Goodness-on-fit on F^2	1.063
Final R indices [$I > 2\sigma(I)$]	R_1 = 0.0980, wR_2 = 0.1874
R indices (all data)	R_1 = 0.1669, wR_2 = 0.2200

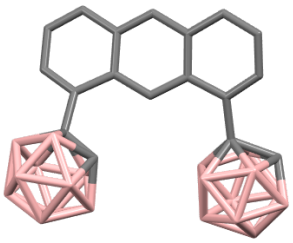

Table S5. Crystallographic data of **1b** (SQUEEZE method was not performed) (CCDC: 2155817)

Empirical formula	$C_{18}H_{30}B_{20}$ • C_4H_5 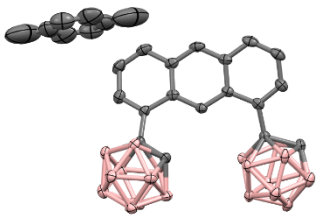
Formula weight	515.70
Temperature (K)	143(2)
Wavelength (Å)	0.71075
Crystal system, space group	monoclinic, $P2_1/c$
Unit cell dimensions	a = 6.926(3)
	b = 28.794(13)
	c = 14.201(7)
	α = 90
	β = 95.438(7)
	γ = 90
V (Å^3)	2819(2)
Z, calculated density (Mg m^{-3})	4, 1.215
Absorption coefficient	0.058
F(000)	1068
Crystal size (mm)	0.17 × 0.09 × 0.01
θ range for data collection	3.038 –27.481
Limiting indices	$-8 \le h \le 8$, $-37 \le k \le 37$, $-18 \le l \le 18$
Reflections collected (unique)	22760/4770 [R(int) = 0.1429]
Goodness-on-fit on F^2	1.098
Final R indices [$I > 2\sigma(I)$]	R_1 = 0.1024, wR_2 = 0.1958
R indices (all data)	R_1 = 0.1814, wR_2 = 0.2340

Computational Methods

The Gaussian 16 program package[8] was used for structural optimization. First, optimized structures of isolated molecules in the ground S_0 states and calculated their electric structures were calculated. The density functional theory (DFT) was applied for the optimization of the structures in the S_0 states at the CAM-B3LYP/6-31G+(d,p) levels. The energy level of the optimized geometry was confirmed to be the local minima by performing frequency calculations and obtaining only positive frequencies.

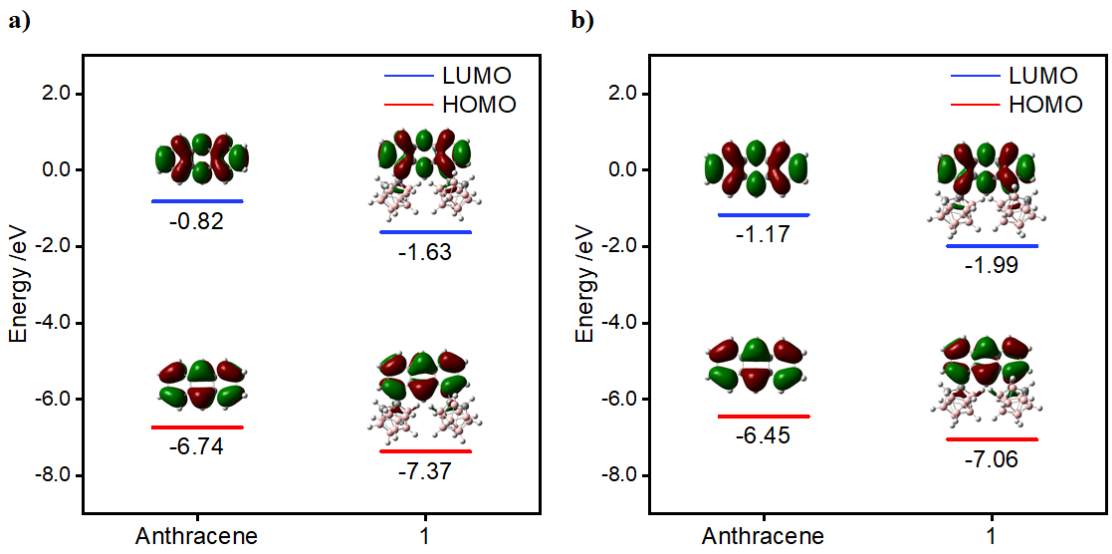

Figure S7. Molecular orbital distribution and energy levels of HOMO and LUMO of anthracene and **1** a) in the ground state calculated with DFT calculation b) in the excited state with TD-DFT calculation.

Table S6. Optimized geometry of **1** in the S_0 state

Center Number	Atomic Number	Coordinates (Angstroms)		
		x	y	z
1	6	-3.52562	1.973791	0.968185
2	6	-2.50777	1.2122	0.458062
3	6	-1.21159	1.849565	0.246476
4	6	-1.16689	3.283502	0.351537
5	6	-2.29246	4.023975	0.81815
6	6	-3.42717	3.374346	1.175061
7	6	-2.9E-05	1.183251	-1.6E-05
8	6	-0.00003	3.9528	-8E-06
9	6	1.166831	3.283503	-0.35154
10	6	1.21154	1.849562	-0.2465
11	6	2.507736	1.212216	-0.45803
12	6	3.52563	1.973829	-0.96803
13	6	3.427174	3.374384	-1.1749
14	6	2.292421	4.023991	-0.81808
15	1	-3.4E-05	0.110565	-5E-06
16	1	-4.47569	1.522259	1.216411
17	1	-2.20699	5.102539	0.905135
18	1	-4.28067	3.910369	1.575272
19	1	-2.6E-05	5.039143	0.000002
20	1	4.475732	1.522316	-1.21616
21	1	4.280706	3.910421	-1.57503
22	1	2.206946	5.102555	-0.90507
23	6	2.816852	-0.22849	-0.07347
24	5	1.891283	-1.58302	-0.52737
25	5	2.01112	-1.07608	1.17164
26	5	3.038538	-2.90483	-0.79133
27	5	3.443636	-1.27273	-1.30319
28	5	2.143504	-2.78668	0.743353
29	1	0.919903	-1.39461	-1.16483
30	5	3.630158	-0.45077	1.452666
31	1	1.125472	-0.54035	1.730961
32	5	3.225479	-2.0818	1.968571
33	5	3.859998	-3.22282	0.756805

34	5	4.663203	-2.27513	-0.5028
35	1	2.827845	-3.73841	-1.60526
36	6	4.408461	-0.67646	-0.03539
37	1	3.575153	-0.80405	-2.37708
38	1	1.279865	-3.54521	1.027646
39	5	4.776186	-1.77524	1.189912
40	1	3.873036	0.525047	2.068402
41	1	3.142741	-2.32627	3.124407
42	1	4.252247	-4.30107	1.050966
43	1	5.645563	-2.51917	-1.11396
44	1	5.13489	0.076559	-0.29144
45	1	5.835174	-1.67959	1.70714
46	6	-2.81686	-0.2285	0.073461
47	5	-1.89126	-1.58302	0.52733
48	5	-2.01111	-1.07606	-1.17166
49	5	-3.0385	-2.90487	0.791274
50	5	-3.44363	-1.27279	1.303164
51	5	-2.14347	-2.78667	-0.7434
52	1	-0.91989	-1.39458	1.1648
53	5	-3.63016	-0.45076	-1.45268
54	1	-1.12548	-0.5403	-1.73098
55	5	-3.22545	-2.08178	-1.96861
56	5	-3.85995	-3.22284	-0.75688
57	5	-4.66318	-2.27518	0.50275
58	1	-2.8278	-3.73846	1.605182
59	6	-4.40847	-0.6765	0.035373
60	1	-3.57515	-0.80412	2.377062
61	1	-1.2798	-3.54514	-1.02776
62	5	-4.77617	-1.77526	-1.18996
63	1	-3.87305	0.52507	-2.06839
64	1	-3.1427	-2.32623	-3.12445
65	1	-4.25218	-4.30108	-1.05107
66	1	-5.64553	-2.51926	1.113907
67	1	-5.1349	0.076517	0.29142
68	1	-5.83515	-1.67963	-1.70719

Table S7. Optimized geometry of **1** in the S_1 state

Center Number	Atomic Number	Coordinates (Angstroms)		
		x	y	z
1	6	-3.50485	1.932183	1.151239
2	6	-2.47716	1.176542	0.528137
3	6	-1.2193	1.803496	0.307178
4	6	-1.15861	3.240263	0.446326
5	6	-2.23335	3.95934	0.976968
6	6	-3.38836	3.286679	1.383739
7	6	0.000004	1.143578	0.000025
8	6	-1.2E-05	3.90174	0.000003
9	6	1.158588	3.240269	-0.44631
10	6	1.219304	1.803506	-0.30714
11	6	2.477156	1.176559	-0.52811
12	6	3.504825	1.932195	-1.15125
13	6	3.38833	3.286688	-1.38377
14	6	2.23332	3.959347	-0.97698
15	1	0.000009	0.070114	0.000027
16	1	-4.41088	1.442594	1.479634
17	1	-2.14672	5.034321	1.096844
18	1	-4.19803	3.824537	1.864211
19	1	-1.9E-05	4.988523	-0.00001
20	1	4.410852	1.442607	-1.47967
21	1	4.197985	3.824545	-1.86427
22	1	2.146676	5.034325	-1.09688
23	6	2.816235	-0.22796	-0.08211
24	5	1.928539	-1.62813	-0.48035
25	5	2.030421	-1.04754	1.196429
26	5	3.115118	-2.92554	-0.68654
27	5	3.475667	-1.30577	-1.26499
28	5	2.211441	-2.76886	0.840053
29	1	0.951247	-1.48773	-1.12365
30	5	3.630455	-0.3646	1.456945
31	1	1.125367	-0.51569	1.730036
32	5	3.270044	-1.98373	2.037308
33	5	3.94132	-3.15469	0.8748

34	5	4.72091	-2.23655	-0.42114
35	1	2.932675	-3.79779	-1.46604
36	6	4.418844	-0.6272	-0.01991
37	1	3.598546	-0.88037	-2.35806
38	1	1.369334	-3.53978	1.154507
39	5	4.814465	-1.66481	1.250323
40	1	3.843402	0.642943	2.031757
41	1	3.189645	-2.18257	3.202073
42	1	4.362871	-4.20829	1.214204
43	1	5.711595	-2.47877	-1.01942
44	1	5.118747	0.141611	-0.30395
45	1	5.86898	-1.51903	1.764975
46	6	-2.81623	-0.22798	0.082128
47	5	-1.9286	-1.62817	0.480458
48	5	-2.03033	-1.04759	-1.19633
49	5	-3.11522	-2.92555	0.686572
50	5	-3.47578	-1.30576	1.264978
51	5	-2.21142	-2.76891	-0.83995
52	1	-0.95135	-1.48778	1.12384
53	5	-3.63033	-0.36462	-1.45699
54	1	-1.12522	-0.51578	-1.72988
55	5	-3.26991	-1.98377	-2.0373
56	5	-3.94131	-3.15469	-0.87483
57	5	-4.72098	-2.23652	0.421034
58	1	-2.93286	-3.79779	1.466106
59	6	-4.41884	-0.62718	0.019812
60	1	-3.59873	-0.88034	2.35803
61	1	-1.36931	-3.53985	-1.15432
62	5	-4.81439	-1.6648	-1.25044
63	1	-3.84321	0.642918	-2.03183
64	1	-3.18942	-2.18263	-3.20205
65	1	-4.36286	-4.20829	-1.21425
66	1	-5.71172	-2.4787	1.019241
67	1	-5.11875	0.14165	0.303783
68	1	-5.86886	-1.519	-1.76518

Table S8. Optimized geometry of anthracene in the S_0 state

Center Number	Atomic Number	Coordinates (Angstroms)		
		x	y	z
1	6	3.649237	0.713305	-1.7E-05
2	6	2.47425	1.403008	0.000041
3	6	1.218694	0.717403	0.000031
4	6	1.218695	-0.7174	0.000014
5	6	2.474251	-1.40301	-1.7E-05
6	6	3.649238	-0.7133	-5.5E-05
7	6	0	1.397752	0.000025
8	6	0.000001	-1.39775	0.000019
9	6	-1.2187	-0.7174	0.000019
10	6	-1.2187	0.717403	0.000009
11	6	-2.47425	1.403008	-2.7E-05
12	1	-2.47125	2.489229	-6.7E-05
13	6	-3.64924	0.713304	-5.1E-05
14	6	-3.64924	-0.7133	-5E-06
15	6	-2.47425	-1.40301	0.00003
16	1	-5E-06	2.484891	0.000042
17	1	4.594667	1.246202	-4.2E-05
18	1	2.471249	2.489229	0.000093
19	1	2.471249	-2.48923	-2.2E-05
20	1	4.594664	-1.24621	-0.00011
21	1	-4E-06	-2.48489	0.000038
22	1	-4.59466	1.246206	-8.1E-05
23	1	-4.59466	-1.24621	-1.7E-05
24	1	-2.47125	-2.48923	0.000074

Table S9. Optimized geometry of anthracene in the S_1 state

Center Number	Atomic Number	Coordinates (Angstroms)		
		x	y	z
1	6	3.689008	-0.69255	0.000003
2	6	2.469942	-1.39457	0.000002
3	6	1.24206	-0.71988	0.000001
4	6	1.24206	0.719879	0
5	6	2.469942	1.394566	0
6	6	3.689008	0.692546	0.000002
7	6	0	-1.39493	0
8	6	0	1.394931	-2E-06
9	6	-1.24206	0.719879	-1E-06
10	6	-1.24206	-0.71988	0
11	6	-2.46994	-1.39457	0
12	1	-2.47388	-2.48061	0
13	6	-3.68901	-0.69255	-1E-06
14	6	-3.68901	0.692546	-1E-06
15	6	-2.46994	1.394566	-2E-06
16	1	0	-2.48214	0
17	1	4.624701	-1.24137	0.000004
18	1	2.473875	-2.48061	0.000003
19	1	2.473875	2.480611	-1E-06
20	1	4.624701	1.241372	0.000002
21	1	0	2.482135	-3E-06
22	1	-4.6247	-1.24137	0
23	1	-4.6247	1.241372	-2E-06
24	1	-2.47388	2.480611	-2E-06

Table S10. Result of TD-DFT calculation for **1** in the S_0 geometry

Excited State	Energy / eV	Wavelength / nm	*f*	Composition	Coefficient
1	3.4598	358.35	0.1511		
				HOMO -> LUMO	0.69810
2	4.0036	309.68	0.0000		
				HOMO–1 -> LUMO	0.48819
				HOMO -> LUMO+1	0.46649
				HOMO -> LUMO+2	0.16267
3	4.7064	263.44	0.1739		
				HOMO–2 -> LUMO	-0.28093
				HOMO–1 -> LUMO	0.16854
				HOMO -> LUMO+1	-0.35424
				HOMO -> LUMO+2	0.49848

Table S11. Result of TD-DFT calculation for **1** in the S_1 geometry

Excited State	Energy / eV	Wavelength / nm	*f*	Composition	Coefficient
1	2.8582	433.78	0.1446		
				HOMO -> LUMO	-0.70447
2	3.7532	330.34	0.0005		
				HOMO–1 -> LUMO	-0.48259
				HOMO -> LUMO+1	-0.33138
				HOMO -> LUMO+2	0.37481
3	4.3322	286.19	0.1058		
				HOMO–2 -> LUMO	0.23507
				HOMO–1 -> LUMO	-0.13361
				HOMO -> LUMO+1	0.55846
				HOMO -> LUMO+2	0.31313

Table S12. Result of TD-DFT calculation for anthracene in the S_0 geometry

Excited State	Energy / eV	Wavelength / nm	*f*	Composition	Coefficient
1	3.6298	341.57	0.0866		
				HOMO–1 -> LUMO+1	-0.11278
				HOMO -> LUMO	0.69847
2	4.0970	302.62	0.0005		
				HOMO–1 -> LUMO	0.50189
				HOMO -> LUMO+1	0.48496
3	5.1981	238.52	0.0000		
				HOMO–2 -> LUMO	-0.42249
				HOMO -> LUMO+5	0.55892

Table S13. Result of TD-DFT calculation for anthracene in the S_1 geometry

Excited State	Energy / eV	Wavelength / nm	*f*	Composition	Coefficient
1	3.0701	403.85	0.0896		
				HOMO -> LUMO	0.70514
2	3.8885	318.85	0.0000		
				HOMO–1 -> LUMO	0.49383
				HOMO -> LUMO+1	0.49309
3	4.8563	255.30	0.0000		
				HOMO–2 -> LUMO	-0.46005
				HOMO -> LUMO+3	-0.53015

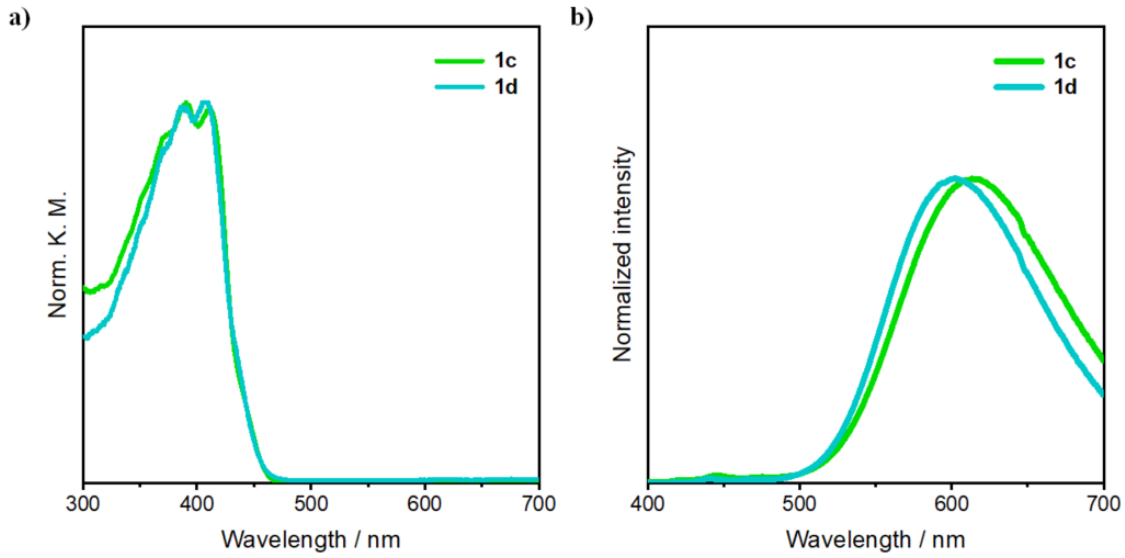

Figure S8. a) Diffusion reflectance and b) PL spectra of **1c** and **1d**.

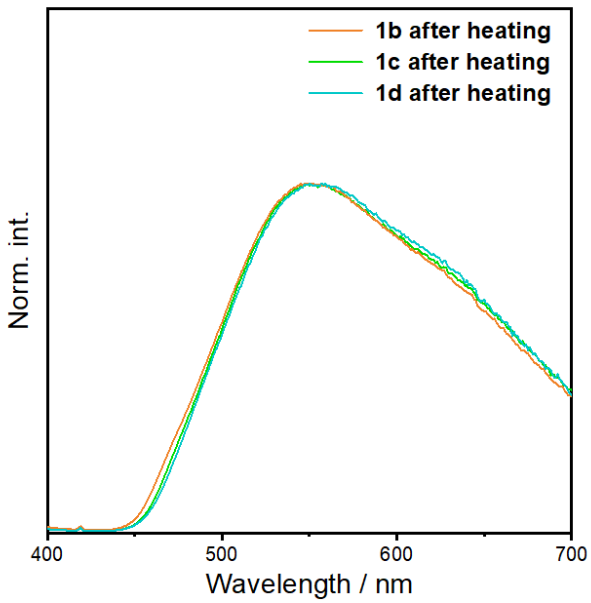

Figure S9. PL spectra of **1b–1d** after heating

Table S14. Photophysical properties of **1** in the crystalline state

Sample	$\lambda_{PL,max}$ / nm[a]	τ / ns[b,c]	Φ[a]
1a	553	53 (89.20%), 16 (10.80%)	0.23
1b	608	11	0.69
1b[d]	548	42 (90.54%), 14 (6.65%), 0.28 (2.81%)	0.23
1c	613	10 (71.45%), 4.6 (28.55%)	0.44
1c[d]	557	42 (90.04%), 15 (9.96%)	0.26
1d	602	12	0.65
1d[d]	550	44 (87.97%), 13 (8.20%), 0.28 (3.83%)	0.22

[a]Excited at 382 nm.

[b]Excited at 369 nm.

[c]Detected at $\lambda_{PL,max}$

[d]After heating.

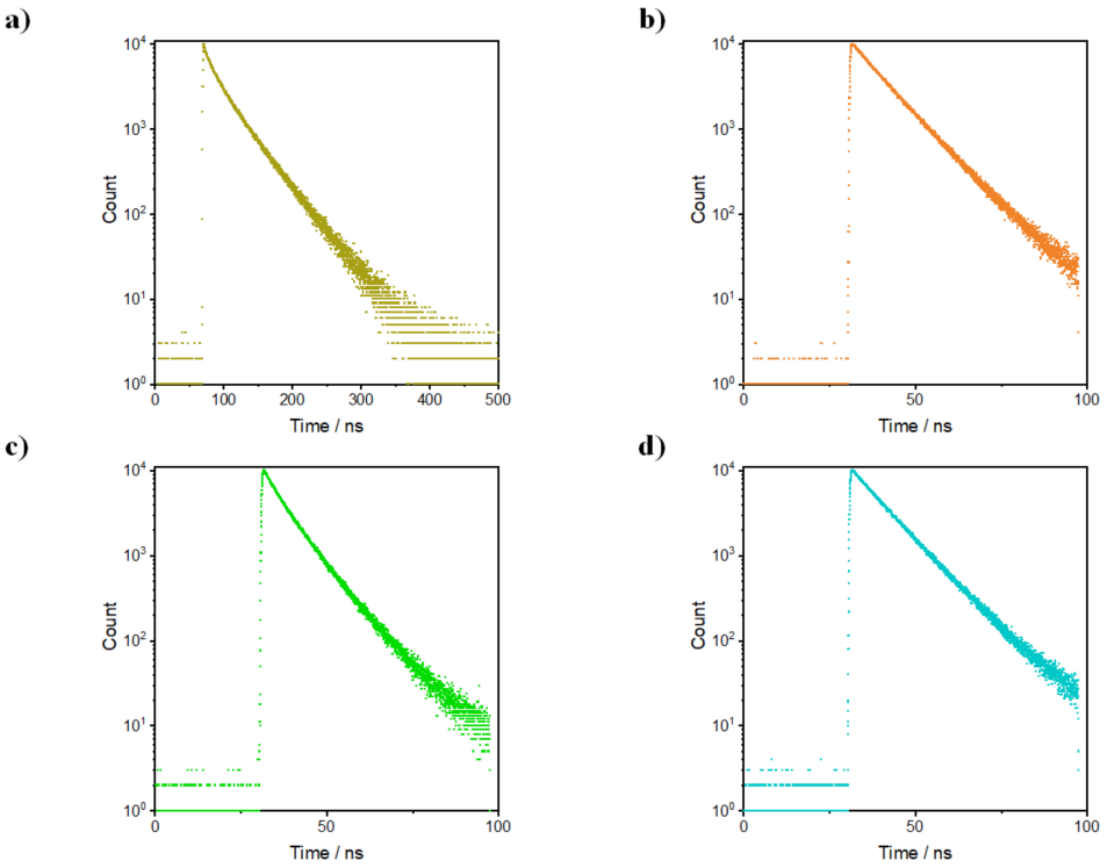

Figure S10. Photoluminescence decay profile of a) **1a**, b) **1b**, c) **1c** and d) **1d** (detected at $\lambda_{PL,max}$ for all samples).

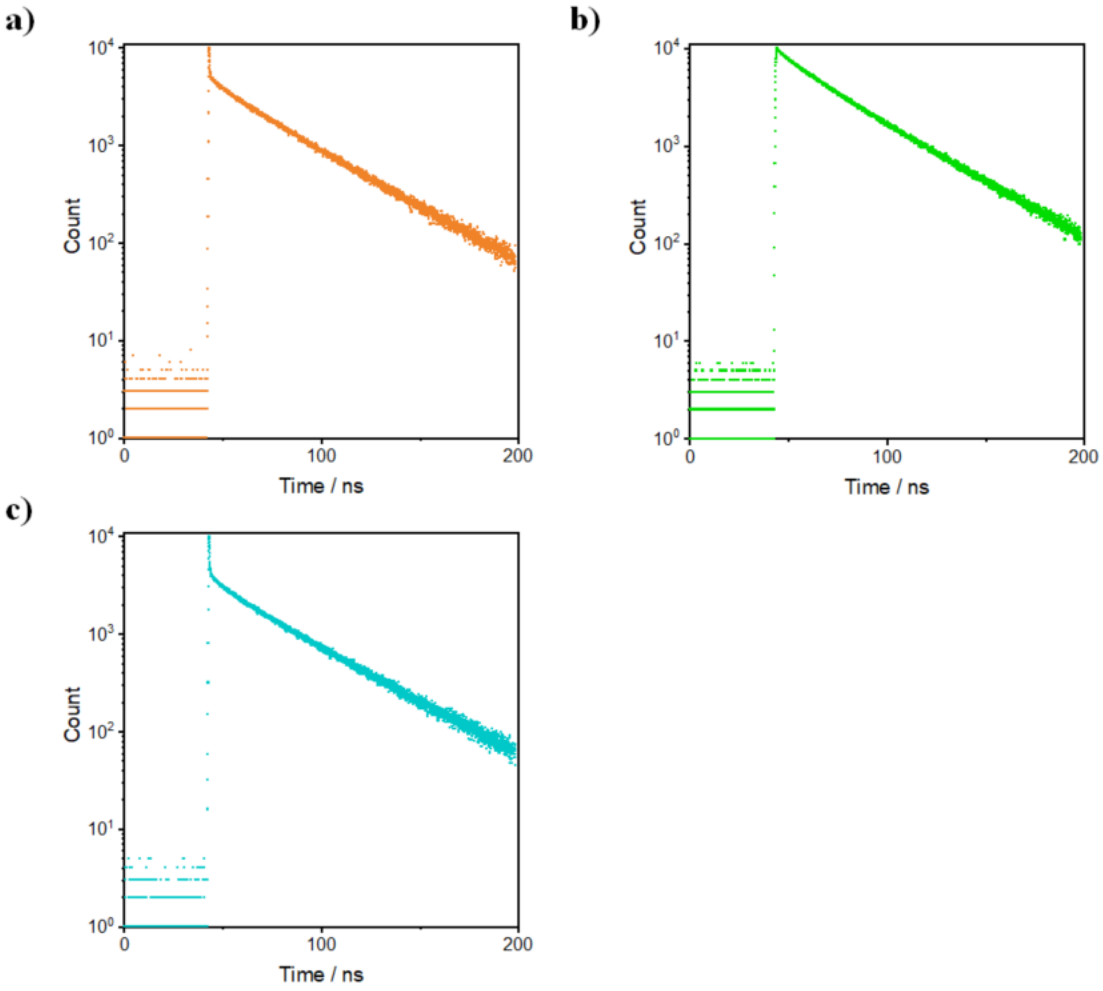

Figure S11. Photoluminescence decay profile of a) **1b**, b) **1c** and c) **1d** after heating (detected at $\lambda_{PL,max}$ for all samples).

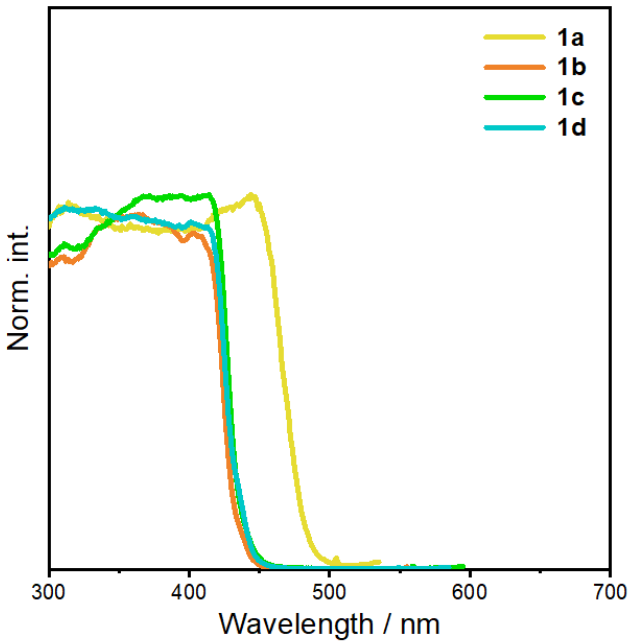

Figure S12. Excitation spectra of **1a–1d**. Detected at $\lambda_{PL,max}$.

Table S15. Photophysical properties of **1** in various solvents[a]

Solvent	λ_{abs} / nm	ε ($M^{-1}cm^{-1}$)	λ_{PL} / nm[b]	τ / ns[c,d]	Φ[b]
Cyclohexane	382	10390	432	n.d.	0.37
			550	6.8	
CCl_4	383	10340	434	n.d.	0.36
			563	7.7	
Toluene	383	9710	435	n.d.	0.42
			610	10	
$CHCl_3$	383	12730	435	n.d.	0.33
			622	9.0	
MeOH	380	10610	431	n.d.	0.06
			675	2.0	

[a] 1.0×10^{-5} M.

[b] Excited at λ_{abs}.

[c] Excited at 369 nm.

[d] Detected at $\lambda_{PL,max}$.

[e] n.d. = not determined due to weak photoluminescence.

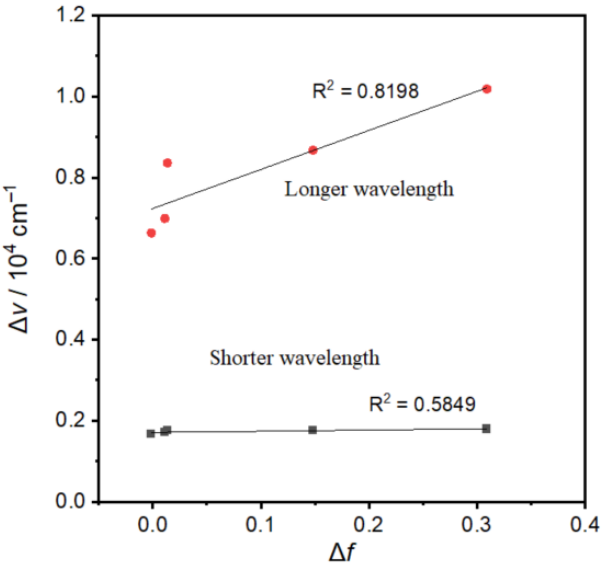

Figure S13. Lippert-Mataga Plot of **1**. The relationship between the solvent polarity parameter (Δf) [a] and stokes shift ($\Delta \nu$)[b] of the absorption and emission maxima.[6–7] [a] $\Delta f = (\varepsilon - 1)/(2\varepsilon+1) - (n^2 - 1)/(2n^2+1)$. [b] $\Delta \nu = \nu_{em} - \nu_{abs}$.

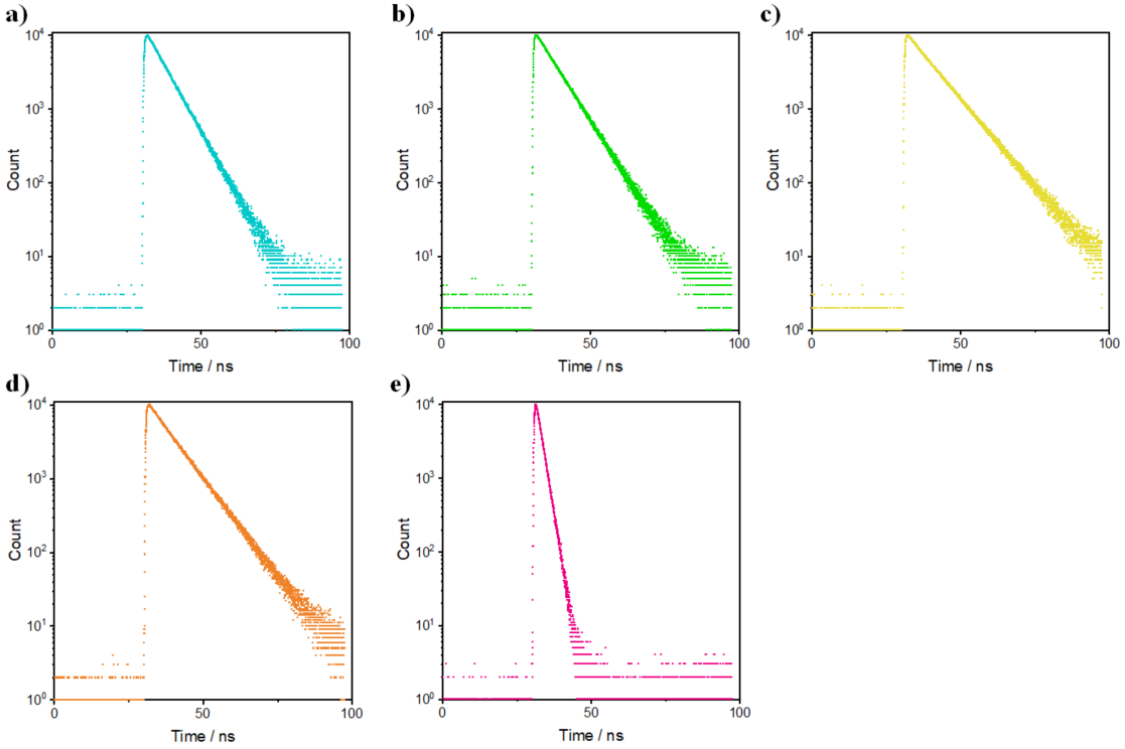

Figure S14. Photoluminescence decay profile of **1** in a) cyclohexane (detected at 550 nm), b) CCl_4 (detected at 563 nm), c) toluene (detected at 612 nm), d) $CHCl_3$ (detected at 622 nm) and e) MeOH (detected at 666 nm).

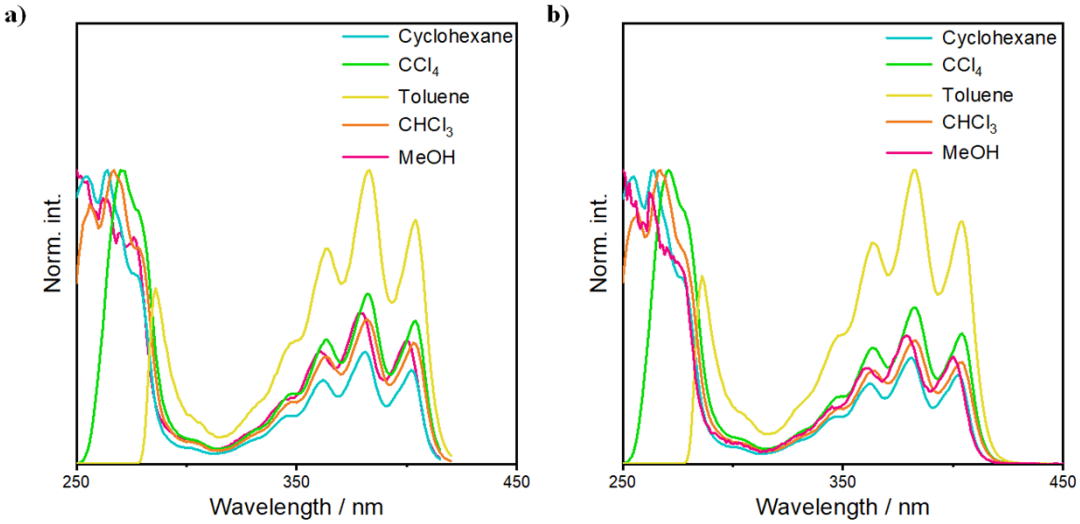

Figure S15. Excitation spectra of **1** in various solvents detected at a) 432 and b) 550 nm for cyclohexane, a) 434 and b) 563 nm for CCl_4, a) 436 and b) 612 nm for toluene, a) 435 and b) 622 nm for $CHCl_3$ and a) 431 and b) 666 nm for MeOH.

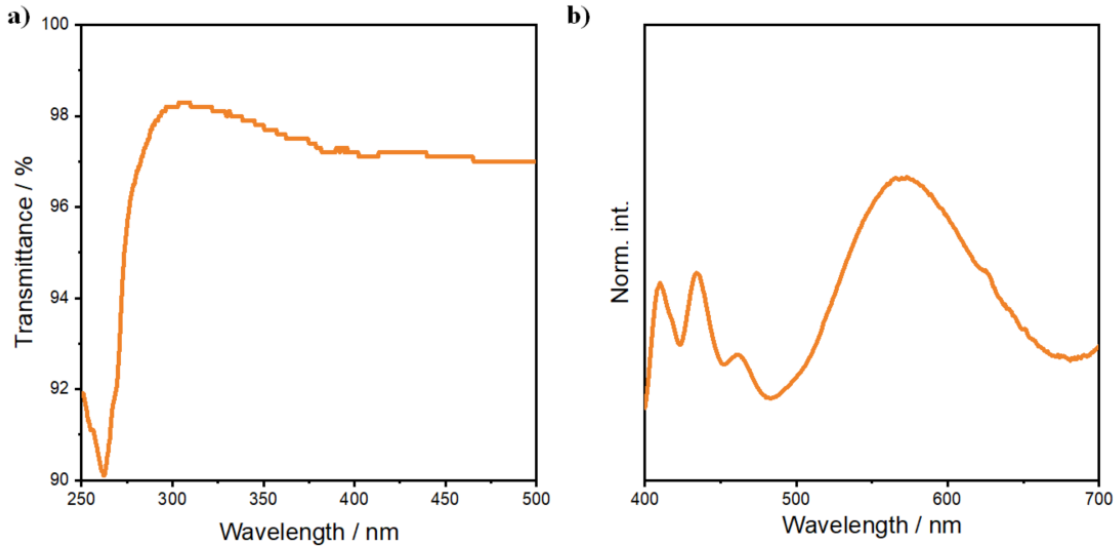

Figure S16. a) UV–vis transmittance and b) PL spectra of **1** dispersed in 1wt% polystyrene film. Film sample was prepared by the spin-coating (1000 rpm, 30 seconds) on the quartz substrate with $CHCl_3$ solution of **1** and polystyrene (1 wt%).

Table S16. Photophysical properties of **1** dispersed in 1wt% polystyrene film

λ_{PL} / nm[a]	τ / ns[b,c]
434	n.d.[d]
573	12 (20.60%), 5.8 (9.75%), 0.14 (69.65%)

[a]Excited at 382 nm.

[b]Excited at 369 nm.

[c]Detected at λ_{PL}.

[d]n.d. = not determined due to weak photoluminescence.

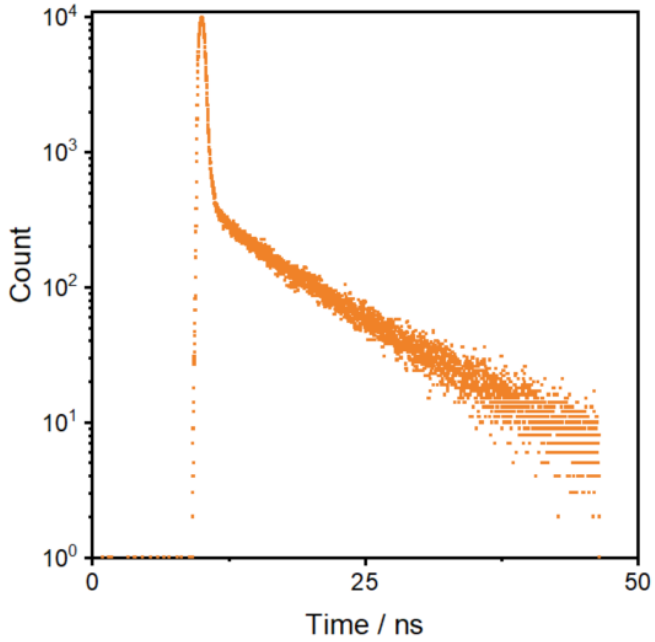

Figure S17. Photoluminescence decay profile of **1** dispersed in 1wt% polystyrene film.

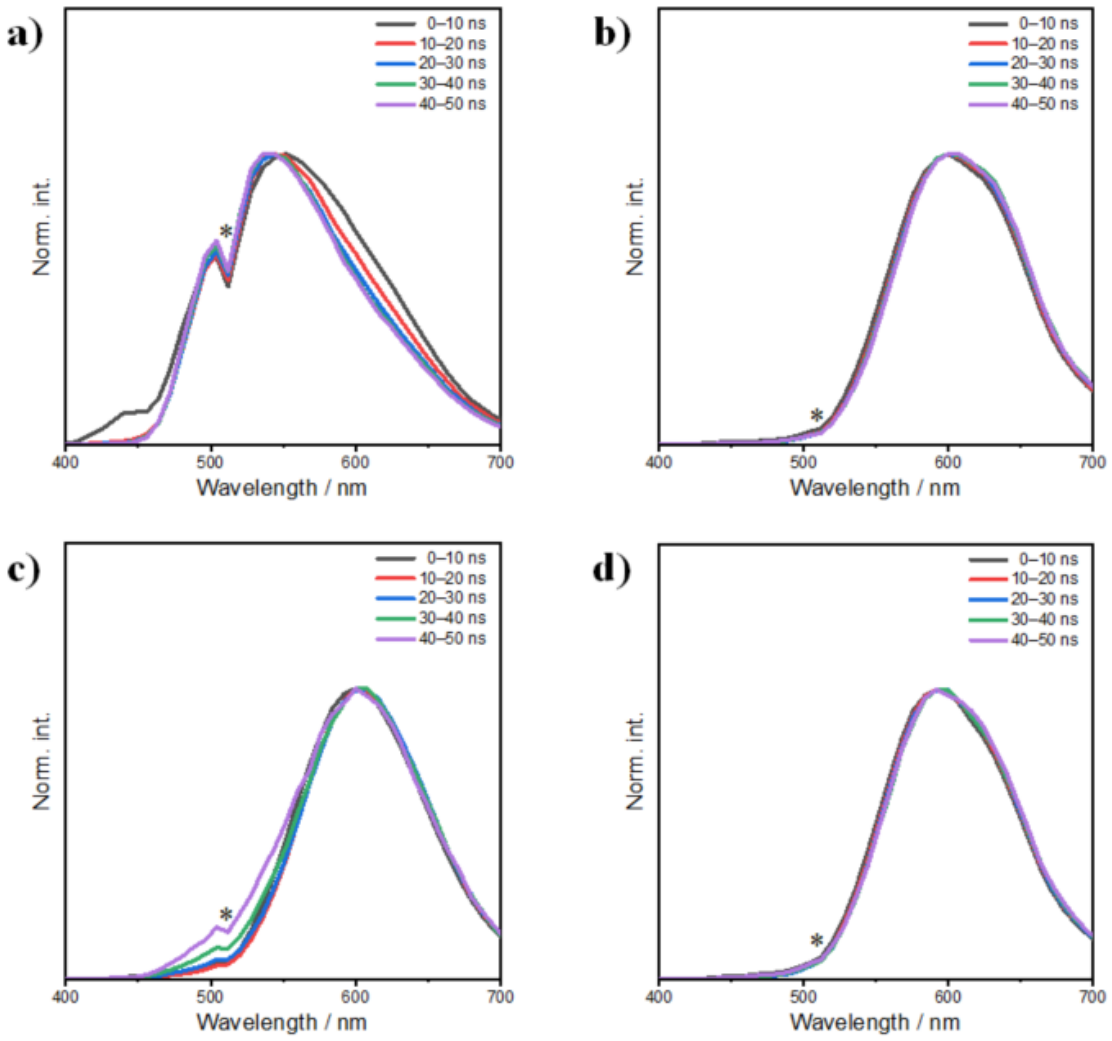

Figure S18. Time resolved emission spectra (TRES) of a) **1a**, b) **1b** c) **1c** and d) **1d**. TRES measurements were performed on 8 nm of detection steps and 60 seconds of integration time. *: noise from instrument setup.

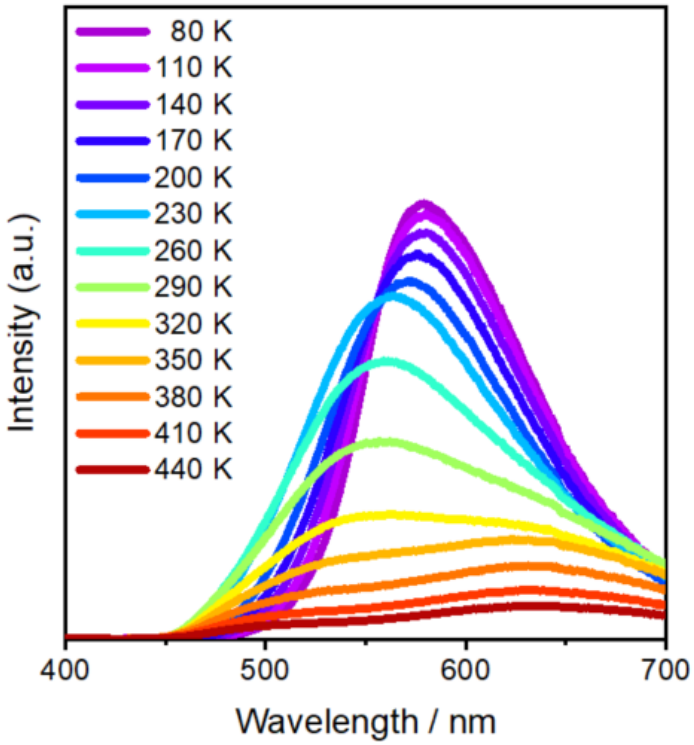

Figure S19. VT-PL spectra of **1b** in 2nd heating from 80 K to 440 K.

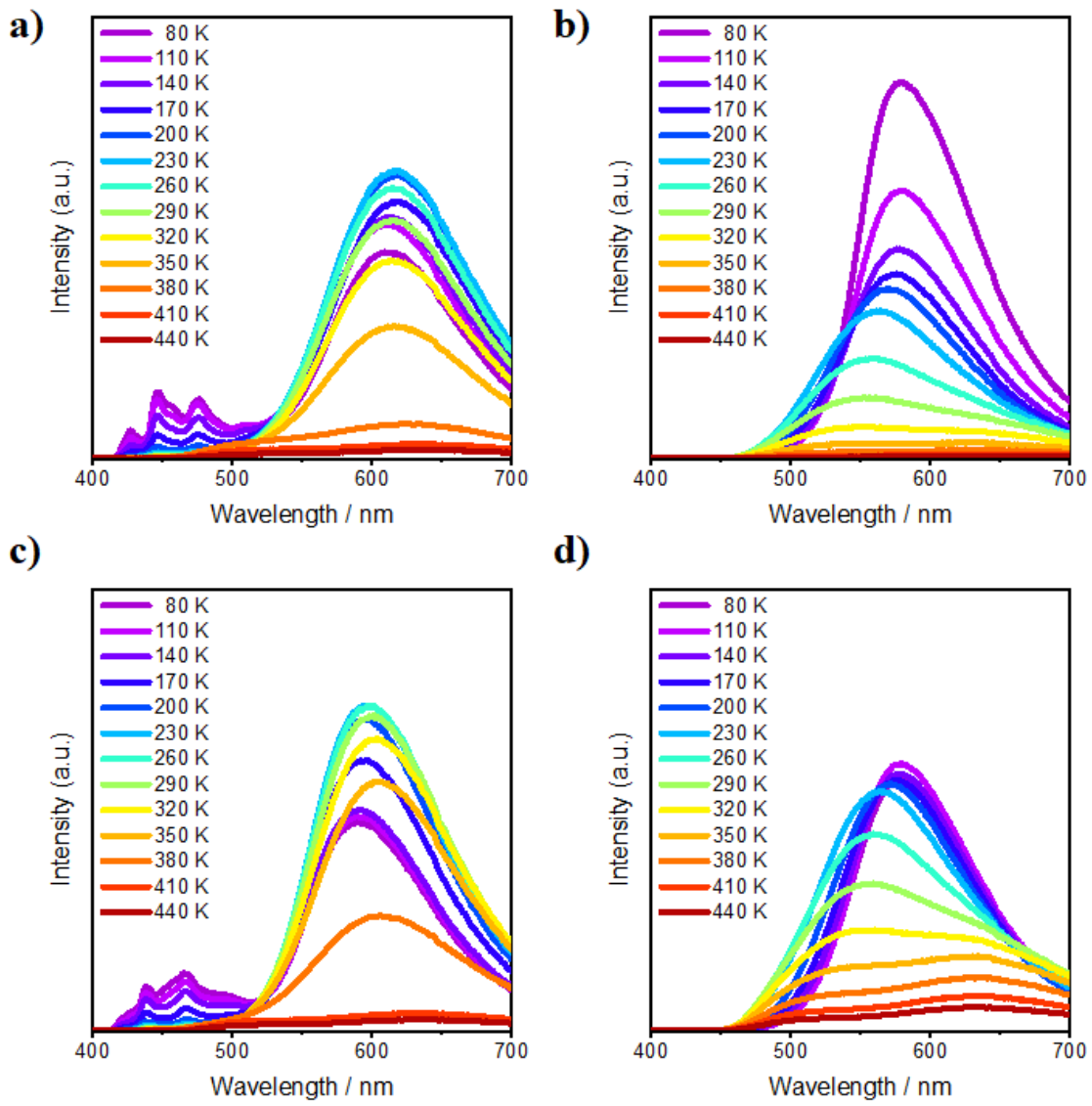

Figure S20. VT-PL spectra of a) **1c** in 1st and b) 2nd heating from 80 K to 440 K and c) **1d** in 1st and d) 2nd heating from 80K to 440 K.

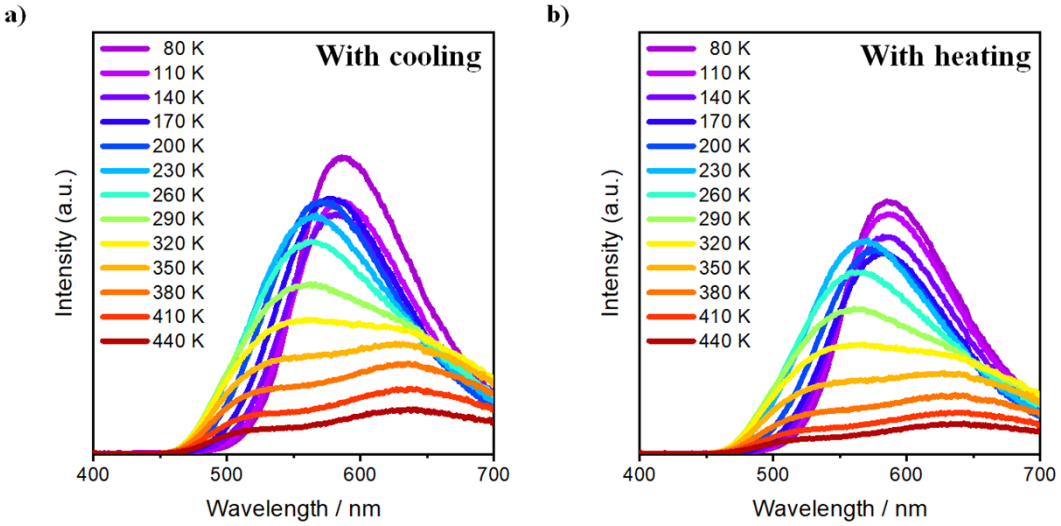

Figure S21. VT-PL spectra of **1a** with a) cooling from 440 K to 80 K, followed by b) heating from 80 K to 440 K.

References

(1) Sheldrick, G. M. *Acta Crystallogr. Sect. A Found. Crystallogr.* **2015**, *71*, 3–8.

(2) Sheldrick, G. M. *Acta Crystallogr. Sect. C Struct. Chem.* **2015**, *71*, 3–8.

(3) Dolomanov, O. V.; Bourhis, L. J.; Gildea, R. J.; Howard, J. A. K.; Puschmann, H. *J. Appl. Crystallogr.* **2009**, *42*, 339–341.

(4) Farrugia, L. J. *J. Appl. Crystallogr.* **1997**, *30*, 565.

(5) Ou, Y. P.; Jiang, C.; Wu, D.; Xia, J.; Yin, J.; Jin, S.; Yu, G. A.; Liu, S. H. *Organometallics* **2011**, *30*, 5763–5770.

(6) Mataga, N.; Kaifu, Y.; Koizumi, M. *Bull. Chem. Soc. Jpn.* **1956**, *29*, 465–470.

(7) Lippert, E. *Berichte der Bunsengesellschaft für physikalische Chemie* **1957**, *61*, 962–975.

(8) Gaussian 16, Revision B.01, M. J. Frisch, G. W. Trucks, H. B. Schlegel, G. E. Scuseria, M. A. Robb, J. R. Cheeseman, G. Scalmani, V. Barone, G. A. Petersson, H. Nakatsuji, X. Li, M. Caricato, A. V. Marenich, J. Bloino, B. G. Janesko, R. Gomperts, B. Mennucci, H. P. Hratchian, J. V. Ortiz, A. F. Izmaylov, J. L. Sonnenberg, D. Williams-Young, F. Ding, F. Lipparini, F. Egidi, J. Goings, B. Peng, A. Petrone, T. Henderson, D. Ranasinghe, V. G. Zakrzewski, J. Gao, N. Rega, G. Zheng, W. Liang, M. Hada, M. Ehara, K. Toyota, R. Fukuda, J. Hasegawa, M. Ishida, T. Nakajima, Y. Honda, O. Kitao, H. Nakai, T. Vreven, K. Throssell, J. A. Montgomery, Jr., J. E. Peralta, F. Ogliaro, M. J. Bearpark, J. J. Heyd, E. N. Brothers, K. N. Kudin, V. N. Staroverov, T. A. Keith, R. Kobayashi, J. Normand, K. Raghavachari, A. P. Rendell, J. C. Burant, S. S. Iyengar, J. Tomasi, M. Cossi, J. M. Millam, M. Klene, C. Adamo, R. Cammi, J. W. Ochterski, R. L. Martin, K. Morokuma, O. Farkas, J. B. Foresman, and D. J. Fox, Gaussian, Inc., Wallingford CT, 2016.